D1-2001-98

# INCLUSIVE PRODUCTION OF HYPERONS IN *n*C INTERACTIONS

Submitted to «European Physical Journal C»

EXCHARM Collaboration:
Dubna — Almaty — Bucharest — Minsk — Moscow — Sofia — Tbilisi

A.N.Aleev, V.P.Balandin, P.Hristov, I.M.Ivanchenko, Z.M.Ivanchenko, M.N.Kapishin, V.D.Kekelidze, Z.I.Kojenkova, V.V.Koren'kov, I.G.Kosarev, N.A.Kuzmin, A.L.Lyubimov, D.T.Madigojine, V.G.Mazny, A.S.Mestvirishvili, N.A.Molokanova, A.N.Morozov, Yu.K.Potrebenikov, L.A.Slepets, V.N.Spaskov, G.T.Tatishvili, I.P.Yudin, N.S.Zaikin, A.I.Zinchenko

*Joint Institute for Nuclear Research, Dubna, Russia*

A.P.Bugorski

*Institute of High Energy Physics, Protvino, Russia*

A.A.Loktionov

*Institute of Physics and Technology, Almaty, Kazakhstan*

T.Ponta, T.Preda

*Institute of Atomic Physics, Bucharest, Romania*

I.M.Geshkov

*Institute for Nuclear Research and Nuclear Energy, Sofia, Bulgaria*

N.S.Amaglobeli, M.V.Kopadze, R.A.Kvatadze, N.L.Lomidze

*High Energy Physics Institute, Tbilisi State University, Georgia*

T.S.Grigalashvili

*Institute of Physics, Georgian Academy of Sciences, Tbilisi, Georgia*

# 1 Introduction

A study of hyperon inclusive production can be a critical test of the models describing quark interaction processes and hadron formation. The existing experimental data on hyperon productions by nucleons were obtained mainly in proton beams [1-19]. There are only few measurements performed in the neutron beams [20, 21]. The existing data do not allow to prove that hyperon production mechanisms in these reactions are equivalent. Thus new results about hyperon production by nucleons and a comparison of hyperon production in neutron and proton beams can provide an additional information for a model of such production.

This paper presents the results on the hyperon inclusive production obtained in the EXCHARM experiment, performed in the neutron beam at the Serpukhov accelerator.

Hyperons were identified by their essential decays:

$$\Lambda^0 \to p\pi^-, \tag{1}$$

$$\begin{aligned}\Sigma(1385)^+ \to\ & \Lambda^0\pi^+ \\ & \hookrightarrow p\pi^-,\end{aligned} \tag{2}$$

$$\begin{aligned}\Sigma(1385)^- \to\ & \Lambda^0\pi^- \\ & \hookrightarrow p\pi^-,\end{aligned} \tag{3}$$

$$\begin{aligned}\Xi^- \to\ & \Lambda^0\pi^- \\ & \hookrightarrow p\pi^-,\end{aligned} \tag{4}$$

$$\begin{aligned}\Xi(1530)^0 \to\ & \Xi^-\pi^+ \\ & \hookrightarrow \Lambda^0\pi^- \\ & \quad \hookrightarrow p\pi^-.\end{aligned} \tag{5}$$

# 2 Experiment EXCHARM

The EXCHARM setup (fig.1) is placed in the neutron beam (channel 5N) of the Serpukhov accelerator. Beam neutrons are produced on the internal beryllium target by 70 GeV primary protons at zero angle to the proton orbit. A lead filter up to 20 cm thick suppresses $\gamma$ contamination in the beam. Accelerator magnets and a special sweeping magnet SP-129 reject

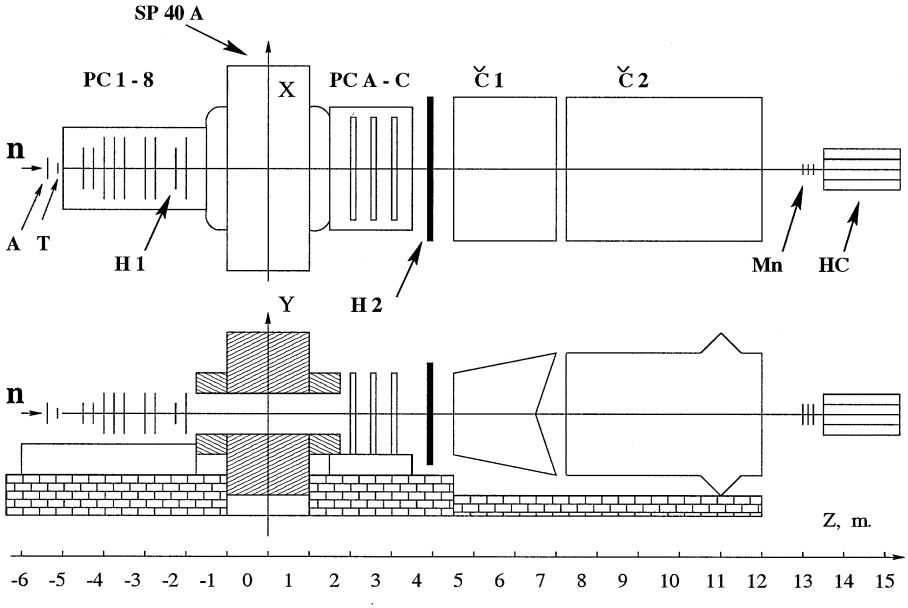


Fig.1. Spectrometer EXCHARM

charged particles from the beam. The neutron energy [22] ranges from 20 GeV to 70 GeV and the mean energy of the beam is $\sim$ 51 GeV (fig.2).

Neutrons are interacting with the target (T) located in front of the spectrometer. The spectrometer analysing dipole magnet SP-40A is used to measure charged particle momenta. The spectrometer is described in the right–handed coordinate system with OZ axis directed along the beam axis, OY directed vertically and with the origin coinciding with the center of the magnet. Charged particles are detected by 11 proportional chambers (25 coordinate planes) with 2 mm wire spacing. 8 chambers upstream the magnet (PC 1-8) have two sensitive planes. Two of them have a wire orientation $\pm 22.5°$ with respect to the vertical plane, others - horizontal and vertical wire orientation. 3 chambers downstream of the magnet (PC A-C) have three sensitive planes each. The wire orientation of three planes are horizontal, vertical and $-22.5°$ with respect to the vertical plane. Hodoscopes of two scitillator counter planes (H1 and H2) and three planes of proportional chambers PC3, PC8 and PCB are included in the trigger system. A more detailed description of the apparatus can be found elsewhere [23].

A carbon target with thickness $L_T$=1.5cm has been used during data taking. The analysing magnet caused a transverse momentum kick of $\sim$ 0.45 GeV/c. The trigger was aimed at selecting events with at least four charged particles passing through the spectrometer. During the run the polarity of the magnetic field has been alternated, then the total statistics was divided approximately into two equal parts with different polarity of the magnetic field.

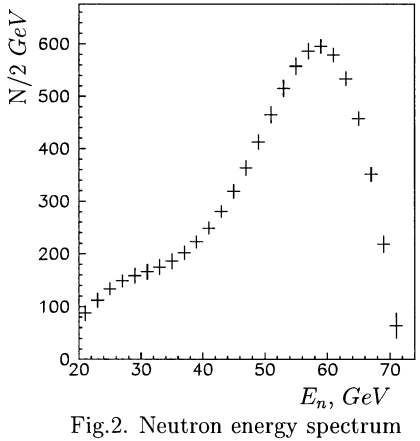

Fig.2. Neutron energy spectrum

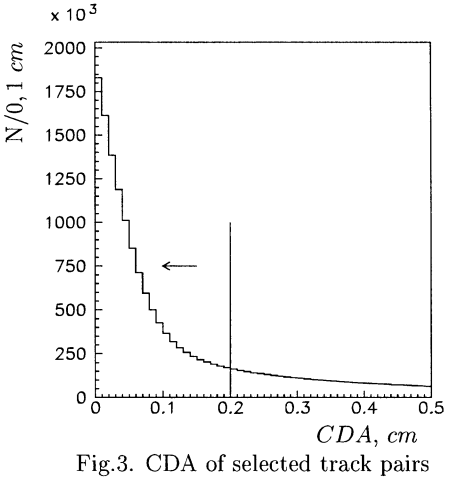

Fig.3. CDA of selected track pairs

The presented results are based on the analysis of $\sim$1.72$\times$10$^8$ recorded events of nC interactions.

# 3 Event selection

The experimental events have been processed by BISON program [24] to reconstruct tracks of charged particles and to define the parameters of these tracks, momenta and charges of corresponding particles. To select the events with different topology and to perform the physical and statistical analysis, the program BISMXC [25] was used.

## 3.1 $\Lambda^0$ identification

Selected events - candidates to (1)–(5) should contain at least a $\Lambda^0$. The decays of $\Lambda^0$ (1) should have a pair of positive and negative particles. A

closest distance of approach (CDA) between tracks of these particles (fig.3) was required to be:

$$CDA < 0.2cm, \tag{6}$$

which corresponds to two experimental resolutions on this parameter. The point, the root-mean-square distance from which to the both tracks was minimal at the closest approach, was considered as a decay vertex. To reduce the background caused by interactions in the target, it was required that Z coordinate of the decay vertex ($Z_\Lambda$) should satisfy the following criterion (fig.4):

$$Z_\Lambda - (Z_T + \frac{1}{2}L_T) > 10cm, \tag{7}$$

where $Z_T$=-460 cm is the coordinate of the target center, Thus, more than 4.5 million pairs were selected.

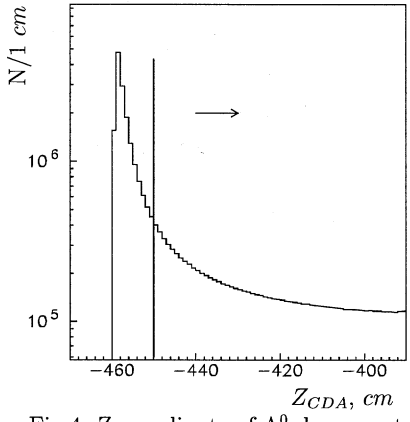


Fig.4. Z coordinate of $\Lambda^0$ decay vertex

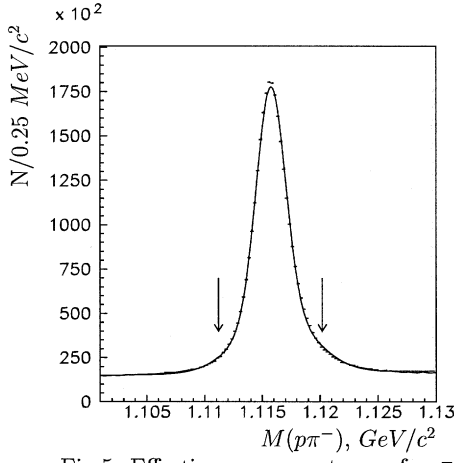


Fig.5. Effective mass spectrum of $p\pi^-$

The $p\pi^-$ effective mass spectrum for the selected pairs of tracks is shown in fig.5. A clear signal of $\Lambda^0$ decay (1) is seen in this spectrum. The background is mainly caused by combinations of the reconstructed charged particles produced in the target ($\approx$ 53%) and ($\approx$ 43%) in the air. The background caused by $K_s^0 \to \pi^+\pi^-$ decays with a positive pion wrongly identified as proton is about 4%. To define the parameters of the signal, the spectrum was approximated by a sum of the Gaussian function describing the signal and a linear function describing the background. The selected pair of tracks was identified as a candidate to $\Lambda^0$ decay, if the corresponding

effective mass $M(p\pi^-)$ was within $\pm 3\sigma_M$ (where $\sigma_M \approx 1.5 MeV/c^2$ is the experimental resolution) of the $\Lambda^0$ nominal mass ($M_{\Lambda^0}$):

$$|M(p\pi^-) - M_{\Lambda^0}| < 4.5 MeV/c^2. \quad (8)$$

The corresponding interval is marked by vertical arrows in fig.5. More than 3 million candidates to $\Lambda^0$ decay (1) have been selected under the criteria (6)–(8) for the following analysis. The real number of $\Lambda^0 \to p\pi^-$ decays has been defined taking into account the linear background.

### 3.2 $\Sigma(1385)^{\pm}$ resonance selection

The candidates to the decays (2) and (3) should contain a reconstructed candidate to $\Lambda^0$ and at least one additional track. The CDA between the $\Lambda^0$ reconstructed trajectory and the additional track which should satisfy the criterion (6), defined a resonance decay vertex. Z coordinate of this vertex should be in the target region, i.e.:

$$(Z_T - \frac{1}{2}T) - 2cm < Z < (Z_T + \frac{1}{2}T) + 2cm. \quad (9)$$

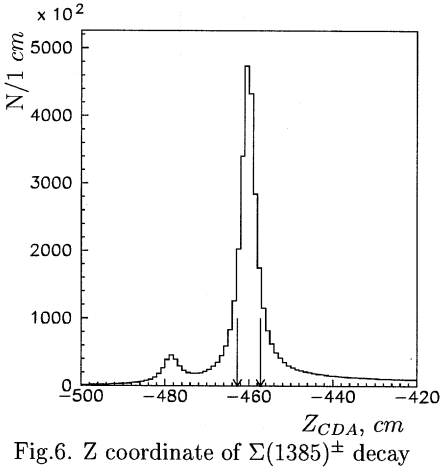


Fig.6. Z coordinate of $\Sigma(1385)^{\pm}$ decay vertex

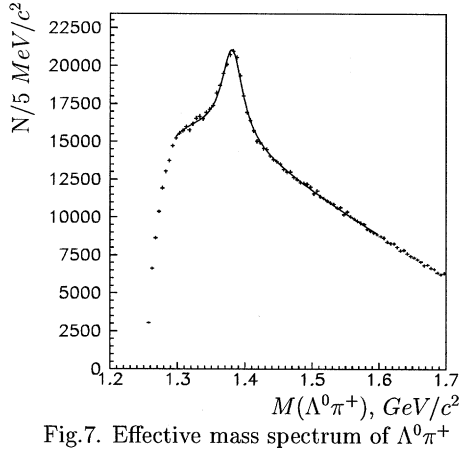


Fig.7. Effective mass spectrum of $\Lambda^0\pi^+$

The corresponding interval has been marked by arrows in fig.6. 2 cm is two experimental resolutions on $Z$. More than 1 million candidates to the decay (2) and slightly less candidates to the decay (3) have been selected. The $\Lambda^0\pi^+$ and $\Lambda^0\pi^-$ effective mass spectra for the selected combinations

are shown in fig's 7 and 8, respectively. Wide signals in these spectra correspond to the decays (2) and (3). These signals have been approximated by the Breit-Wigner function (BW) folded with the normal distribution(G):

$$BWG(M) = A \int G(M-m)BW(m)dm, \tag{10}$$

where

$$G(M-m) = exp(-\frac{(M-m)^2}{2\sigma_M^2}), \tag{11}$$

$$BW(m) = \frac{mM_0\Gamma}{(m^2-M_0^2)^2+M_0^2\Gamma^2}, \tag{12}$$

$A$ is an amplitude, $\sigma_M$ is a mass resolution, $M_0$ is a mass of resonance, $\Gamma$ – its width. Backgrounds have been approximated by the function:

$$BG(m) = P_1(m-M_{th})^{P_2}exp(-P_3m-P_4m^2), \tag{13}$$

where $P_1$ - $P_4$ are free parameters, $M_{th}$ - a sum of masses of decay products. The numbers of detected resonances were defined by integration of obtained functions approximating the signals on the full effective mass spectra. The background was caused mainly by combinatorics.

### 3.3 $\Xi^-$ selection

Selected events for the decay (4) should contain a candidate to $\Lambda^0$ and at least one additional track of the negative particle. The CDA between reconstructed $\Lambda^0$ trajectory and this track should satisfy the criterion (6), forming a $\Xi^-$ decay vertex. $Z$ coordinate of the $\Xi^-$ decay vertex ($Z_\Xi$) should satisfy the following criterion:

$$Z_\Xi - (Z_T + \frac{1}{2}T) > 5cm. \tag{14}$$

To distinguish the $\Lambda^0$ and $\Xi^-$ decay vertices, the distance between them should be greater than 5 cm:

$$Z_\Lambda - Z_\Xi > 5cm. \tag{15}$$

As a result around 150 thousand of such combinations have been selected. The $\Lambda^0\pi^-$ effective mass spectrum of the selected combinations is shown in fig.9.

A clear signal of $\Xi^-$ decay (4) is seen in this spectrum. The spectrum was approximated by a sum of the Gaussian function, describing the signal, and

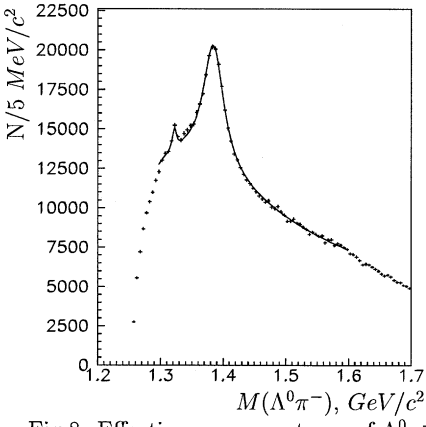


Fig.8. Effective mass spectrum of $\Lambda^0\pi^-$

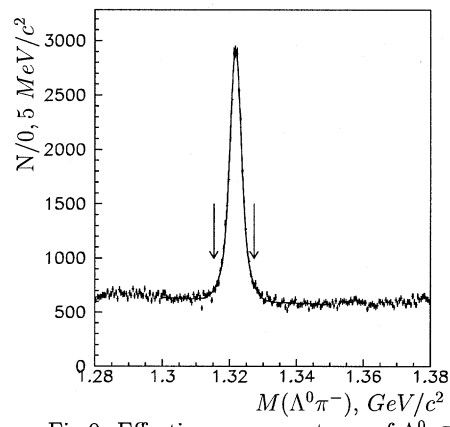


Fig.9. Effective mass spectrum of $\Lambda^0\pi^-$

the linear function, describing the background. The combination was identified as the $\Xi^-$ decay, if the $M(\Lambda^0\pi^-)$ was within $\pm 3\sigma_M$ ($\sigma_M \approx 2.0 MeV/c^2$ is the corresponding mass resolution) of the $\Xi^-$ nominal mass:

$$|M(\Lambda^0\pi^-) - M_{\Xi^-}| < 6.0 MeV, \tag{16}$$

The corresponding interval is marked by vertical arrows in fig.9. Around 37000 candidates to the decay (4) satisfying the criteria (14)–(16) were selected and used for the following analysis. The number of $\Xi^- \to \Lambda^0\pi^-$ decays was defined by subtraction of the background combinations from the selected combinations.

### 3.4 $\Xi(1530)^0$ resonance selection

Selected events for the decay (5) should contain a candidate to $\Xi^-$ and at least one additional track of the positive charged particle. The trajectory of $\Xi^-$ and additional track should satisfy the criterion (6) and $Z$ coordinate should be in the target region, i.e. should satisfy the criterion (9). About 10000 candidates to the decay (5) have been selected. The effective mass spectrum for the selected events is shown in fig.10.

A clear signal of the decay (5) is seen in this spectrum. To define the parameters of the signal, the obtained effective mass spectrum was approximated by a sum of the function (10), describing the signal, and a smooth function (13), describing the background. The number of $\Xi(1530)^0$

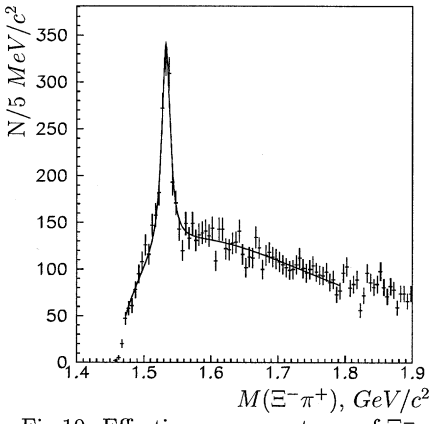


Fig.10. Effective mass spectrum of $\Xi^-\pi^+$

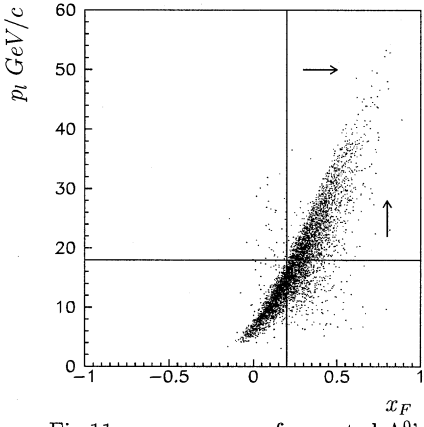


Fig.11. $p_l$ versus $x_F$ of accepted $\Lambda^0$'s.

Table 1. Characteristics of hyperon signals.

| Decay | Mass$[MeV/c^2]$ | $\sigma_M$ $[MeV/c^2]$ | $\Gamma$ $[MeV/c^2]$ | The number of |
|---|---|---|---|---|
| $\Lambda^0 \to p\pi^-$ | $1115.90 \pm 0.01$ | $1.55 \pm 0.01$ | - | $2426800 \pm 1900$ |
| $\Sigma(1385)^+ \to \Lambda^0\pi^+$ | $1380.9 \pm 0.3$ | 3.2 | $35.1 \pm 0.9$ | $69300 \pm 1900$ |
| $\Sigma(1385)^- \to \Lambda^0\pi^-$ | $1384.5 \pm 0.2$ | 3.4 | $40.0 \pm 0.9$ | $97500 \pm 2100$ |
| $\Xi^- \to \Lambda^0\pi^-$ | $1321.8 \pm 0.4$ | $1.97 \pm 0.1$ | - | $21370 \pm 190$ |
| $\Xi(1530)^0 \to \Xi^-\pi^+$ | $1533.3 \pm 0.6$ | 3.7 | $10.0 \pm 1.7$ | $1123 \pm 89$ |

was defined by integration of the function, approximating the signal, on the full effective mass spectrum.

The characteristics of the reconstructed $\Lambda^0$, $\Sigma(1385)^+$, $\Sigma(1385)^-$, $\Xi^-$ and $\Xi(1530)^0$ signals are shown in tab.1.
The corresponding mass resolutions $\sigma_M$'s for resonances have been obtained by Monte Carlo simulation. The measured masses of hyperons are near the corresponding nominal masses [26] and their widths coincide with the nominal ones within the errors.

# 4 Hyperon production characteristics

Monte Carlo (MC) technique was applied to calculate the efficiencies of registration and define the hyperon production characteristics.

The following reactions were simulated:

$$n + N \to \Lambda^0 + K^0 + X,$$
$$n + N \to \Sigma(1385)^+ + K^0 + \pi^- + X,$$
$$n + N \to \Sigma(1385)^- + K^+ + X,$$
$$n + N \to \Xi^- + K^+ + K^0 + X,$$
$$n + N \to \Xi(1530)^0 + K^0 + K^0 + X.$$

Here $K^0$, $K^+$ and $\pi^-$ are the so called "minimum accompanying particles", which compensate strangeness and charges of the studied states; X is a set of particles generated by JETSET [27] in accordance with the conservation laws.

The parametrisation following the quark counting rules [28] has been used to describe the hyperon production models:

$$E\frac{d^3\sigma}{dp^3} \sim \frac{E^*}{p^*}\frac{d^2\sigma}{dx_F dp_t^2} \sim (1 - |x_F|)^n e^{-bp_t^2}, \qquad (17)$$

where $x_F$ is the Feynman variable, $p_t$ - transverse momentum, $E^*$ and $p^*$ - energy and momentum of the particle in the center mass system for the reaction of $nN$ interaction. To obtain n parameter, $x_F$ was varied within the kinematic region: $0.2 < x_F < 1$ for $\Lambda^0$ and $0.1 < x_F < 1$ for other hyperons. The same parametrisation was applied to simulate each accompanying particle but in the whole kinematic region $-1 < x_F < 1$. Since the value of $x_F$ in every experimental event is not known, then to provide the same conditions of the analysis of the experimental and MC data, the cut on $p_l$ has been used, which corresponds to the appropriate region of $x_F$. As an example, the corresponding cuts on $x_F$ and $p_l$ for $\Lambda^0$ are shown in fig.11. GEANT based program [29] was used to trace the particles through the experimental setup. The simulated data were treated by the same reconstruction and analysis programs, which were used to process the experimental data.

To obtain $n$ and $b$ parameters, the normalized $p_l$ and $p_t^2$ spectra of the reconstructed hyperons were approximated by the corresponding MC spectra. The $\chi^2$ criterion was used to estimate the quality of this approximation. The chosen $n$ and $b$ parameters for the studied events correspond to the best approximation of the $p_l$ and $p_t^2$ spectra. As an example the normalized $p_l$ and $p_t^2$ spectra for $\Lambda^0$ at minimal $\chi^2$'s are shown in figs.12 and 13, correspondingly.

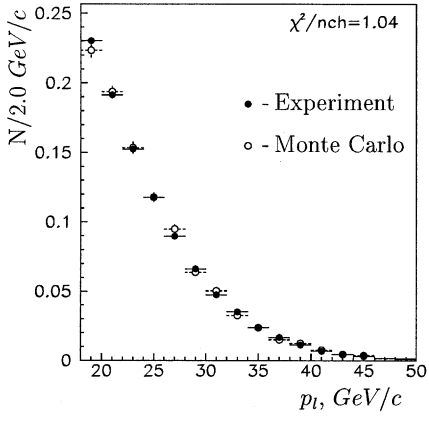


Fig.12. $p_l$ spectra of $\Lambda^0$.

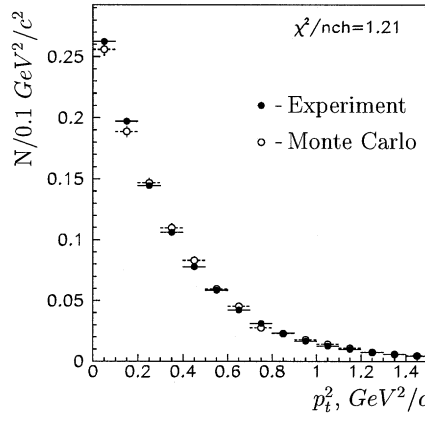


Fig.13. $p_t^2$ spectra of $\Lambda^0$.

The obtained values of the parameters $n$ and $b$ and the corresponding minimal $\chi^2$'s are shown in tab.2. Errors of the parameters were calculated according to the method of multi parameter errors calculating [30]. For example, four free parameters define $\Lambda^0$ production in the used model: $n$ and $b$ describing of $\Lambda^0$ and $n$ and $b$ describing of the accompanying particle ($K^0$). In this case an error of $n$ was defined as a variation of $n$ if the full $\chi^2$ of two normalized $p_l$ spectra – experimental and MC was changed on $\delta\chi^2$=4.88. The value of $\delta\chi^2$ depends on the number of free parameters and was defined by the following consideration: the probability for the selected parameter to be within its error, was equal to 70 %. Correlations between $n$ and $b$ were not taken into account.

Table 2. Production parameters of hyperons.

| State | n | $\chi^2_{p_l}/nch$ | b | $\chi^2_{p_t^2}/nch$ |
|---|---|---|---|---|
| $\Lambda^0$ | $2.1 \pm 0.1$ | 1.04 | $2.4 \pm 0.1$ | 1.21 |
| $\Sigma(1385)^+$ | $2.7 \pm 0.1$ | 0.64 | $1.8 \pm 0.1$ | 0.56 |
| $\Sigma(1385)^-$ | $1.3 \pm 0.1$ | 1.03 | $1.9 \pm 0.1$ | 0.89 |
| $\Xi^-$ | $4.0 \pm 0.1$ | 0.53 | $2.0 \pm 0.1$ | 0.43 |
| $\Xi(1530)^0$ | $3.2 \pm 0.2$ | 0.38 | $2.1 \pm 0.2$ | 0.77 |

The parameters $n$ measured for $\Sigma^{\pm}$ and $\Xi(1530)^0$ are compatible with the

Table 3. Number of hyperon decays and efficiencies of the their detection.

| Decay | $p_l[GeV/c]$ | Number of | $\epsilon_{tot} \cdot 10^2$ |
|---|---|---|---|
| $\Lambda^0 \to p\pi^-$ | $> 18$ | $1075800 \pm 1400$ | $2.027 \pm 0.021$ |
| $\Sigma(1385)^+ \to \Lambda^0\pi^+$ | $> 12$ | $68400 \pm 1400$ | $1.641 \pm 0.031$ |
| $\Sigma(1385)^- \to \Lambda^0\pi^-$ | $> 12$ | $95200 \pm 2100$ | $1.629 \pm 0.032$ |
| $\Xi^- \to \Lambda^0\pi^-$ | $> 12$ | $19390 \pm 280$ | $1.378 \pm 0.017$ |
| $\Xi(1530)^0 \to \Xi^-\pi^+$ | $> 12$ | $1096 \pm 84$ | $0.610 \pm 0.014$ |

predictions of the quark counting model ($n$=1 for $\Sigma(1385)^-$ and $n$=3 for $\Sigma(1385)^+$ and $\Xi(1530)^0$) [28], but the parameters $n$ obtained for $\Lambda^0$ and $\Xi^-$ are higher than the predicted ones ($n$=1 for $\Lambda^0$ and $n$=3 for $\Xi^-$).

## 5 Cross-section measurement

The inclusive production cross-sections of the hyperons were calculated by the following formula:

$$\sigma_{nC} = \frac{N_s \cdot A_c}{M_n \cdot N_a \cdot S \cdot \epsilon \cdot BR},$$

where $BR$ - the decay branching ratio of the considered state; $N_s$ - the number of combinations in the signal; $A_c$ - the target nucleus atomic weight; $M_n$ - the number of neutrons having passed through the target ($M_n = (2.31 \pm 0.13) \cdot 10^{11}$); $N_a$ - Avogadro constant; $S = 1.3 g/cm^2$ - the target thickness; $\epsilon$ - the efficiency of the decay detection.

$N_s$ were defined as the values of signals in the effective mass spectra of corresponding hyperon decays, obtained at the corresponding criteria on $p_l$. The obtained values of $N_s$ and $\epsilon$ are shown in tab.3.

The calculated cross-sections of the hyperon inclusive production on carbon nucleus ($\sigma_{nC}$) are presented in tab.4.

Systematic errors include an error of $M_n$, errors of registration efficiencies and errors, defined by the errors of the model parameters. The last error was calculated as a quadratic sum of $\sigma_{nC}$ variations at different values of the parameters $n$ and $b$ within their errors. Possible correlation effects are not taken into account.

The total cross-sections have been calculated using the following assumptions:

Table 4. Cross sections of the hyperon production.

| State | $x_F$ | $\sigma_{nC}[\mu b]$ | | | | |
|---|---|---|---|---|---|---|
| $\Lambda^0$ | $> 0.2$ | 5511 | $\pm$ | $7(stat)$ | $\pm$ | $460(syst)$ |
| $\Sigma(1385)^+$ | $> 0.1$ | 492 | $\pm$ | $10(stat)$ | $\pm$ | $31(syst)$ |
| $\Sigma(1385)^-$ | $> 0.1$ | 690 | $\pm$ | $15(stat)$ | $\pm$ | $65(syst)$ |
| $\Xi^-$ | $> 0.1$ | 146 | $\pm$ | $2(stat)$ | $\pm$ | $9(syst)$ |
| $\Xi(1530)^0$ | $> 0.1$ | 28 | $\pm$ | $2(stat)$ | $\pm$ | $4(syst)$ |

- The $x_F$ dependence of $\Lambda^0$ differential cross-section in the region $0 < x_F < 0.2$ are the same that in the work [31].
- The $x_F$ dependences of the differential cross-sections for other hyperons under consideration in the region of $0 < x_F < 0.1$ are the extrapolations to this region of the measured dependences.
- The $x_F$ dependences of the differential cross-sections are symmetrical relative to $x_F = 0$.

To calculate the cross-sections on nucleon ($\sigma_{nN}$), the following dependence: $\sigma_{nC} = \sigma_{nN} \cdot A^{2/3}$ was assumed. The obtained cross-sections are shown in tab.5. The shown errors were calculated as quadratic sums of the corresponding statistical and systematic errors.

Table 5. Total cross-sections of the hyperon production.

| State | $\sigma_{nC}[\mu b]$ | | | $\sigma_{nN}[\mu b]$ | | |
|---|---|---|---|---|---|---|
| $\Lambda^0$ | 17400 | $\pm$ | 1500 | 3330 | $\pm$ | 280 |
| $\Sigma(1385)^+$ | 1453 | $\pm$ | 96 | 277 | $\pm$ | 18 |
| $\Sigma(1385)^-$ | 1770 | $\pm$ | 170 | 337 | $\pm$ | 33 |
| $\Xi^-$ | 496 | $\pm$ | 31 | 95 | $\pm$ | 6 |
| $\Xi(1530)^0$ | 87 | $\pm$ | 14 | 17 | $\pm$ | 3 |

To compare the obtained results with the data of proton experiments, the measured cross-sections were recalculated taking into account the following relations based on the additive quark model:

$$\sigma_{pp}(\Lambda^0) \approx \sigma_{pN}(\Lambda^0) \approx \sigma_{nN}(\Lambda^0),$$

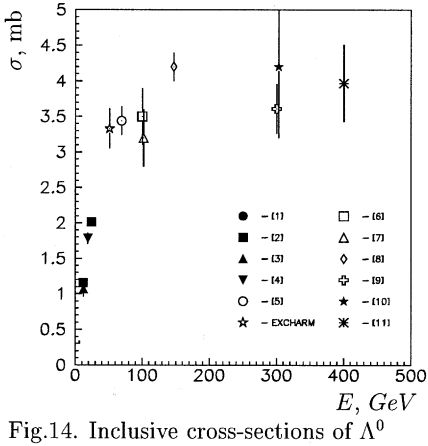


Fig.14. Inclusive cross-sections of $\Lambda^0$

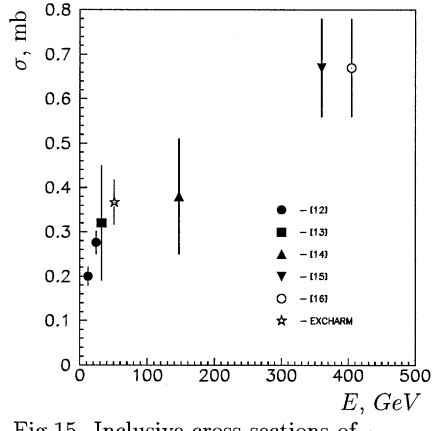


Fig.15. Inclusive cross-sections of $\Sigma(1385)^+$

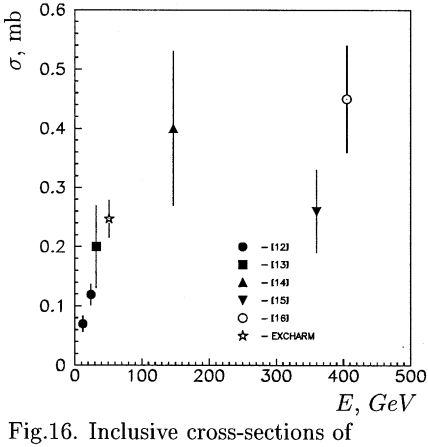


Fig.16. Inclusive cross-sections of $\Sigma(1385)^-$

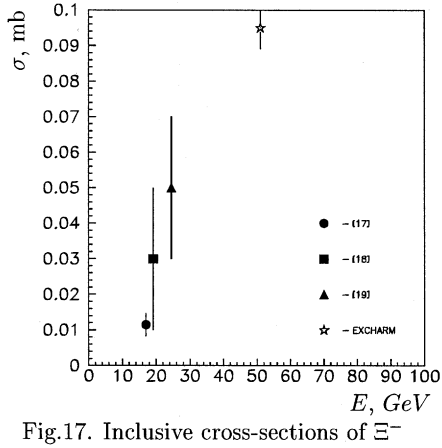


Fig.17. Inclusive cross-sections of $\Xi^-$

$$\sigma_{pp}(\Sigma(1385)^+) \approx \frac{3}{2}\sigma_{nN}(\Sigma(1385)^-) - \frac{1}{2}\sigma_{nN}(\Sigma(1385)^+),$$
$$\sigma_{pp}(\Sigma(1385)^-) \approx \frac{3}{2}\sigma_{nN}(\Sigma(1385)^+) - \frac{1}{2}\sigma_{nN}(\Sigma(1385)^-),$$
$$\sigma_{pp}(\Xi^-) \approx \sigma_{pN}(\Xi^-) \approx \sigma_{nN}(\Xi^-),$$

which leads to:

$$\sigma_{pp}(\Lambda^0) = (3330 \pm 280)\mu b,$$
$$\sigma_{pp}(\Sigma(1385)^+) = (367 \pm 50)\mu b,$$
$$\sigma_{pp}(\Sigma(1385)^-) = (247 \pm 33)\mu b,$$
$$\sigma_{pp}(\Xi^-) = (95 \pm 6)\mu b.$$

The calculated values and data of other experiments are shown in figs.14–17. One can see that the cross-sections of $\Lambda^0$, $\Sigma(1385)^-$, $\Sigma(1385)^+$ and $\Xi^-$ produced in neutron and proton beams are very close.

## 6 Summary

The total cross-sections of the inclusive production of hyperons in neutron-carbon interactions at the mean neutron energy $\sim 51GeV$ have been measured (tab.5). The measured cross-sections of $\Lambda^0$ and $\Xi^-$ production include the ones of $\Lambda^0$ and $\Xi^-$ produced due to decays of resonances and cascade decays. The calculated $\sigma_{pp}$ for $\Lambda^0$, $\Sigma(1385)^+$, $\Sigma(1385)^-$ and $\Xi^-$ coincide with the measured ones in the proton experiments.

The widths of resonances $\Sigma(1385)^+$, $\Sigma(1385)^-$ and $\Xi(1530)^0$ have been measured (tab.1).

Parameters $n$ and $b$ of the used parametrisation (17) have been defined (tab.2).

Authors are greatly indebted to A.N.Sissakian and N.E.Tyurin for their permanent support of this investigations, to C.Cheshkov – for valuable discussion.

This work is supported by the Russian Foundation for Basic Research, project 00-07-90148.

## References

[1] R.L. Eisner et al. *Nucl.Phys.*, B123 (1977) 361.

[2] H. Fesefeldt et al. *Nucl.Phys.*, B147 (1979) 317.

[3] K. Jaeger et al. *Phys.Rev.*, D11 (1975) 1756.

[4] H. Boggild et al. *Nucl.Phys.*, B57 (1973) 77.

[5] D. Blumenfeld et al. *Nucl.Phys.*, B125 (1977) 253.

[6] M. Alston et al. *Phys.Rev.Lett.*, 35 (1975) 142.

[7] J.W. Chapman et al. *Phys.Lett.*, 47B (1973) 465.

[8] D. Brick et al. *Nucl.Phys.*, B164 (1980) 1.

[9] A. Sheng et al. *Phys.Rev.*, D11 (1975) 1733.

[10] F.T. Dao et al. *Phys.Rev.Lett.*, 30 (1973) 1151.

[11] R.D. Kass et al. *Phys.Rev.*, D20 (1979) 605.

[12] K. Bockmann et al. *Nucl.Phys.*, B143 (1978) 395.

[13] K. Bogolyubsky et al. *Sov.J.Nucl.Phys*, 50 (1989) 424.

[14] D.Brick et al. *Phys.Rev.*, D25 (1982) 2248.

[15] T. Aziz et al. *Z.Phys*, C30 (1986) 381.

[16] H. Kichimi et al. *Phys.Rev*, D20 (1979) 37.

[17] R.E. Ansorge et al. *Nucl.Phys.*, B103 (1976) 509.

[18] K. Alpgard et al. *Nucl.Phys.*, B103 (1976) 234.

[19] J. Bartke et al. *Nuovo.Cim.*, 29 (1963) 8.

[20] A.N. Aleev et al. *Yad.Fiz.*, 44 (1986) 661.

[21] M.I. Adamovich at al. *Z.Phys C*, 76 (1997) 35.

[22] A.N.Aleev et al. *JINR preprint* P13-94-312 (Dubna, 1994).

[23] A.N. Aleev et al. *Instrum.Exp.Tech.*, 42 (1999) 481.

[24] A. Boniushkina et al. *JINR preprint* P1-93-168 (Dubna, 1993).

[25] A.I. Zinchenko et al. *IFVE AN RK*, 92-01 (Alma-Ata, 1992).

[26] Review of Particle Physics. *Eur.Phys.Jour.*, C15 (2000).

[27] T.Sjöstrand *Computer Physics Commun.*, 82 (1994) 74.

[28] J.F. Gunion *Phys.Lett.*, 88B (1979) 150.

[29] G.A. Aralbaeva et al. *JINR preprint*, P1-93-85 (Dubna, 1993)

[30] F. James *Minuit Reference Manual*, D506 (CERN, 1994).

[31] A.B.Kaidalov, O.I.Piskunova *Z.Phys. C*, 30 (1986) 145.

Received by Publishing Department
on May 17, 2001.

Алеев А.Н. и др. Д1-2001-98
Инклюзивное рождение гиперонов в $n$C-взаимодействиях

Измерены сечения инклюзивного рождения гиперонов $\Lambda^0$, $\Xi^-$ и гиперонных резонансов $\Sigma(1385)^{\pm}$, $\Xi(1530)^0$ в нейтрон-углеродных взаимодействиях при средней энергии нейтронов ~ 51 ГэВ. Определены экспериментальные значения параметров использованной параметризации дифференциального сечения $\left(1-|x_F|\right)^n e^{-bp_t^2}$, где $x_F$ — переменная Фейнмана, $p_t$ — поперечный импульс. Проведено сравнение полученных результатов с предсказаниями модели кваркового счета и результатами других экспериментов.

Работа выполнена в Лаборатории физики частиц ОИЯИ при поддержке Российского фонда фундаментальных исследований, проект № 00-07-90148.

Препринт Объединенного института ядерных исследований. Дубна, 2001

Aleev A.N. et al. D1-2001-98
Inclusive Production of Hyperons in $n$C Interactions

Inclusive production cross-sections of hyperons $\Lambda^0$, $\Xi^-$ and hyperon resonances $\Sigma(1385)^{\pm}$, $\Xi(1530)^0$ have been measured in neutron–carbon interactions at ~ 51 GeV mean energy of neutrons. The experimental parameter values of used differential cross-section parametrization $\left(1-|x_F|\right)^n e^{-bp_t^2}$, where $x_F$ is Feynman variable, $p_t$ is transverse momentum, have been defined. The obtained results have been compared with the predictions of quark counting rules and existing experimental data.

The investigation has been performed at the Laboratory of Particle Physics, JINR, and supported by the Russian Foundation for Basic Research, Project No. 00-07-90148.

Preprint of the Joint Institute for Nuclear Research. Dubna, 2001

Макет Т.Е.Попеко

Подписано в печать 07.06.2001
Формат 60 × 90/16. Офсетная печать. Уч.-изд. листов 1,8
Тираж 305. Заказ 52687. Цена 2 р. 16 к.

Издательский отдел Объединенного института ядерных исследований
Дубна Московской области